Magnetism of sperimagnetic amorphous RCo_3 thin films with R = Dy, Tb, and Tm

Zexiang Hu,[1] Ajay Jha,[1] Katarzyna Siewierska,[2] Simon Lenne,[1] Pierre le Berre,[3] Nora M. Dempsey,[3] Plamen Stamenov,[1] Karsten Rode,[1] and J. M. D. Coey[1,*]

[1]*School of Physics and Centre for Research on Adaptive Nanostructures and Nanomaterials, Trinity College Dublin, Dublin D02 PN40, Ireland*

[2]*Institute for Methods and Instrumentation for Synchrotron Radiation Research, Helmholtz-Zentrum Berlin für Materialen und Energie GmbH, Albert-Einstein-Strasse 15, 12489 Berlin, Germany*

[3]*Université Grenoble Alpes, CNRS, Grenoble INP, Institut Néel, 38000 Grenoble, France*

(Received 5 January 2024; accepted 11 June 2025; published 22 July 2025)

The magnetization of amorphous sputtered films of a-R_xCo_{1-x}, with $x \approx 0.25$ and R = Dy, Tb, or Tm, is investigated by magnetometry, anomalous Hall effect, and magneto-optic Kerr effect to understand how the magnetic structure of the films is influenced by temperature and the quadrupole and higher multipole moments of the rare-earth charge distribution. Square magnetic hysteresis loops with perpendicular magnetic anisotropy and divergent coercivity that reaches 3.5 T in the vicinity of the compensation temperature T_{comp} are observed at 175 and 200 K for Dy and Tb films, respectively, but the coercivity in Tm films never exceeds 0.5 T and shows no divergence near the compensation at 50 K. The temperature dependence of the net rare-earth moment is inferred from the cobalt moment of soft ferromagnetic a-Y_xCo_{1-x}. The magnitude of the second-order random anisotropy energy exceeds the antiparallel R-Co exchange coupling for all three rare earths. The negative quadrupole moments of Dy and Tb lead to random easy-axis anisotropy with large coercivity. The positive quadrupole moment of Tm favors random hard-axis anisotropy where each Tm has an easy plane. The resulting sperimagnetic ground states are modeled by a distribution of rare-earth moments within a cone of half-angle θ_0 whose axis is antiparallel to the ferromagnetic axis of cobalt. The reduced moment $\langle J_z\rangle/J$ at $T = 0$ is calculated from a one-atom Hamiltonian as a function of α, the ratio of uniaxial anisotropy to exchange energy per rare-earth atom for different angles θ between the local anisotropy axis, and the ferromagnetic Co axis. Extrapolated values of $\langle J_z\rangle/J$ are ~0.75 at low temperature for both Dy and Tb, with a sharp increase <10 K attributed to higher-order multipole moments. The hard-axis random anisotropy resulting from the positive quadrupole moment of Tm leads to a larger low-temperature value of $\langle J_z\rangle/J = 0.84$. On increasing temperature, the magnitude of the rare-earth moment and the local random anisotropy that creates the sperimagnetism are reduced; the cone angle narrows, but the noncollinear structure persists well above room temperature for Dy but not for Tb, a difference related to the opposite signs of their hexadecapole moments. A temperature-dependent spin-flop field observed near compensation in a-$Dy_{25}Co_{75}$ extrapolates to 2.0 T at T_{comp}, a remarkably low value that is associated with the nonrigid character and high transverse susceptibility of the frustrated Dy subnetwork. An x-ray photoemission electron microscopy investigation of partial single-pulse all-optical switching in a 10 nm a-$Dy_{25}Co_{75}$ film as a function of temperature establishes that the process is stochastic, and unrelated to inhomogeneities in the films. The size of the sperimagnetic domains in the unmagnetized state is ~200 nm, <300 K.

DOI: 10.1103/yzfd-jqvx

I. INTRODUCTION

Interest in the magnetism of amorphous alloys of rare earths with iron or cobalt dates back to work in the 1970s and 1980s on crystalline rare-earth intermetallic compounds, which were studied in an effort to understand the relevant exchange and crystal-field interactions [1,2]. That research, which led to the discovery of $Nd_2Fe_{14}B$ [3], was spurred by a demand for cobalt-free permanent magnets in the aftermath of the 1976 cobalt crisis when the best permanent magnets, Sm-Co and Alnico, were both Co based. Metal evaporation and sputtering techniques were then being perfected to produce thin films of the amorphous counterparts. A wealth of experimental information was acquired on their magnetism [4], and a classification scheme for the collinear and noncollinear amorphous magnetic structures was proposed [5]. An early focus was to develop perpendicular media for magneto-optical data recording [6] based on Curie point or compensation point writing, for which amorphous ferrimagnetic $Gd_{0.25}Fe_{0.656}Co_{0.094}$ films were optimized [7]. They were later found to exhibit helicity-dependent all-optical switching [8], and repetitive single-pulse all-optical toggle

*Contact author: jcoey@tcd.ie

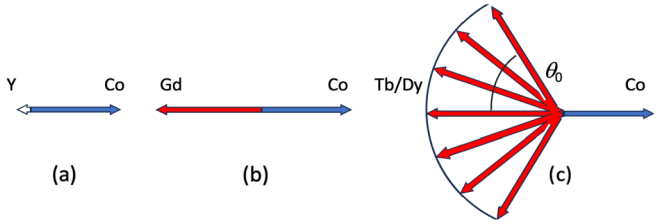

FIG. 1. Schematic magnetic structures of amorphous alloys: (a) ferromagnetic a-YCo_3 and (b) ferrimagnetic a-$GdCo_3$, and (c) sperimagnetic a-$DyCo_3$.

switching independent of photon helicity (SPAOS) discovered in 2012 [9] was a fast thermal response of the film to irradiation with subpicosecond laser pulses. The same effect is found in binary amorphous a-$Gd_{0.30}Co_{0.70}$ films [10] but not in Gd-free a-$Dy_{0.25}Co_{0.75}$ or a-$Tb_{0.25}Co_{0.75}$ films, where partial single-pulse all-optical switching is observed only for the first few pulses [11]. (In this paper "a-" is used to denote an amorphous alloy). Complete one-shot switching of a-$Tb_{0.24}Co_{0.76}$ could be achieved in microdots with microantennas [12] or in a 1.5 T bias field [13].

The amorphous alloys of Co with a heavy rare earth Gd, Tb, Dy, Ho, Er, or Tm have a ferrimagnetic compensation point T_{comp} below or close to room temperature when the ratio of rare-earth (R) to Co is ∼1:3 [4,7,14–17]; the compensation can be tuned by varying the rare-earth content x in a-R_xCo_{1-x}. Although Gd alloys are collinear ferrimagnets [7,14], Dy atoms in a-$DyCo_3$ were shown by ^{161}Dy Mossbauer spectroscopy to adopt a noncollinear structure at low temperature [17] related to the random local electrostatic fields acting on the electric quadrupole moment of the incomplete Dy $4f$ shell, which produces local random easy-axis anisotropy. The resulting noncollinear ferrimagnetism, known as *sperimagnetism*, was modeled by a uniform distribution of rare-earth moment orientations within a cone of half-angle θ_0 aligned antiparallel to the cobalt magnetization direction (Fig. 1). We recently reported that amorphous alloys of Co with Y, a nonmagnetic rare earth, are soft ferromagnets, with negligible hysteresis [18].

Recent studies of a-R_xCo_{1-x} films, R = Gd, Tb, Dy, relevant to the present work include investigations of the sperimagnetism [19–21], determinations of the atomic moments by x-ray magnetic circular and linear dichroism [22,23], reports of a bulk Dzyaloshinskii-Moriya interaction in a-GdFeCo [24], and a skyrmion lattice in $DyCo_3$ [25,26]. More generally, there has been a recent revival of interest in these materials in the context of ferrimagnetic spintronics [27], where ultrafast longitudinal spin dynamics in the picosecond range underpins all-optical switching, and large anisotropy fields in the vicinity of T_{comp} facilitate fast transverse spin dynamics and high-speed domain-wall propagation.

As a prelude to reinvestigating the magnetism of the amorphous R-Co alloys with a heavy rare earth, we examined the magnetism of the a-Y_xCo_{1-x} series [18], where yttrium serves as a nonmagnetic proxy for the $4f$ rare earths. Lanthanum $4f^0$ has also been used in this context [19]. Films with a wide range of composition $0 < x \leqslant 0.55$ covered the appearance of magnetism at $x = 0.5$. A focus on compositions with $x \approx 0.25$, an Y:Co ratio of 1:3, where the volumes occupied by Y and Co atoms in the structure are almost equal, revealed that the cobalt in a-$Y_{0.25}Co_{0.75}$ has a large orbital moment of 0.31 μ_B and a random local anisotropy of 5.2 K/atom (3.2 MJ m^{-3}), yet the alloy is a soft ferromagnet because of anisotropy averaging in the Co exchange field [18]. The Co-Co exchange is greater in the amorphous state than it is in the crystalline state, and the Curie temperature of pure amorphous cobalt (if it existed) has been predicted to be ≈2000 K [28,29]. The ratio of exchange energy to local anisotropy energy of a Co atom in a-$Y_{0.25}Co_{0.75}$ is 220. We show here that exchange averaging is ineffective for heavy rare-earth alloys because of the much stronger local random easy- or hard-axis anisotropy of the $4f$ atoms and the weaker exchange field acting on the rare earth, which tends to follow the local easy directions for Dy and Tb and avoid the local hard directions for Tm, leading to distinct coercivity and random noncollinear magnetic structures.

All three amorphous rare-earth cobalt systems are sperimagnets, but there are substantial differences related to the sign of the $4f$ quadrupole moment, which we explain. These include the narrower angular dispersion and larger reduced moment of Tm, its modest coercivity that does not diverge at compensation, as it does for Tb and Dy, and the large transverse susceptibility of the rare-earth subnetwork after spin flop near compensation. The role of higher-order terms in the random local crystal field acting on the rare earth is discussed. By *local crystal field*, we mean the local electrostatic field acting on a particular $4f$ atom.

II. THIN FILMS

A first series of films of a-R_xCo_{1-x}, with R = Dy or Tb and $x \approx 0.25$, were grown in Dublin on oxidized silicon wafers by DC sputtering from separate 50 mm rare-earth and cobalt targets using a Shamrock sputtering system with a base pressure of ∼8 × 10^{-8} Torr. No metallic Pt or Ta underlayer or overlayer was used. Films were capped with a 2–4-nm-thick layer of SiO_2 or Al_2O_3 to protect them from oxidation. Tb and Dy were chosen because they are the heavy rare earths with the largest negative quadrupole moments [30], which are needed for local easy-axis anisotropy in the amorphous R-Co_3 atomic environment. Film composition was chosen to favor perpendicular net anisotropy and ensure that compensation occurs below room temperature where the ferromagnetic magnetization of the cobalt subnetwork is practically temperature independent. The concentration x was determined from the calibrated deposition rates from the individual targets. Films were characterized by wide- and small-angle x-ray scattering using a Philips Panalytical X'pert Pro diffractometer and reflectivity software to determine the thicknesses, roughness, and density of the film and cap layers [18]. Films were characterized magnetically by superconducting quantum interference device (SQUID) magnetometry, magneto-optic Kerr effect (MOKE), and anomalous Hall effect (AHE) measured by the van der Pauw method.

A difference noted between a-Dy_xCo_{1-x} and a-Tb_xCo_{1-x} is that the Dy films were stable in ambient conditions for a year or more, whereas the Tb films began to deteriorate after about a month. This may be related to the different oxides associated with the two rare earths. Dy forms a sesquioxide

TABLE I. Room-temperature structural and magnetic data on the first series of amorphous thin films.

Number	Chemical formula	Main layer thickness (nm)	Main layer roughness (nm)	Main layer density (g/cm^3)	Capping layer	Capping layer thickness (nm)	Capping layer roughness (nm)	M_s (kA/m)	T_{comp} (K)	H_s (kA/m)	H_c (mT)
1	$Dy_{0.25}Co_{0.75}$	10.3	1.2	9.2	SiO_2	3.3	0.9	173.0	180	–	48.2
2	$Dy_{0.25}Co_{0.75}$	8.8	1.0	9.0	AI_2O_3	3.2	1.0	148.5	175	–	73.0
3	$Dy_{0.25}Co_{0.75}$	10.5	1.6	8.2	SiO_2	4.6	0.8	223.0	200	–	33.6
4	$Tb_{0.25}Co_{0.75}$	17.1	1.6	8.0	SiO_2	4.5	1.5	106.0; 26.8[a]	200	–	295.9
5	$Tb_{0.25}Co_{0.75}$	20.0	1.7	7.2	SiO_2	4.6	0.8	120.0; 50.7[a]	180	–	253.6
6	$Tb_{0.20}Co_{0.80}$	19.7	0.6	8.6	AI_2O_3	1.5	0.5	375.0	20	–	34.0
7	$Y_{0.25}Co_{0.75}$	8.8	1.0	6.5	SiO_2	2.0	0.8	705.4		647.0	<1.0
8	$Y_{0.25}Co_{0.75}$	19.0	1.3	6.5	SiO_2	2.0	1.5	721.7		598.4	<1.0

[a]Anhysteretic soft component.

like most other trivalent lanthanides, but Tb forms a higher oxide Tb_4O_7, which is a mixture of phases containing trivalent $4f^8$ and quadrivalent $4f^7$ terbium ions [31]. Data on the materials of most interest from the first series are listed in Table I, including two a-$Y_{0.25}Co_{0.75}$ films for comparison [18].

The a-$Tm_{0.25}Co_{0.75}$ film reported here was grown by RF magnetron sputtering (Alliance Concept—DP850) in Grenoble. Tm was selected because it has a large atomic moment, like Dy or Tb, but a positive quadrupole moment which favors local hard-axis/easy-plane anisotropy in the amorphous environment. The film, of thickness 89 nm, was grown on an oxidized Si wafer and capped with a Ta layer of thickness 2.2 nm. The thickness of the layers was determined by profilometry performed on reference samples. The magnetic properties were characterized by SQUID-VSM magnetometry, and no Bragg reflections from Co or any *R*-Co intermetallic phases were seen by x-ray scattering in any of the diffraction patterns except for pure Co in the first series.

III. RESULTS

Our initial focus here is on films exhibiting square magnetization loops and perpendicular magnetic anisotropy.

A. Dysprosium alloys

The first series of amorphous a-$Dy_{0.25}Co_{0.75}$ alloys was prepared with a range of thickness from 5 to 94 nm, and magnetization was measured both parallel and perpendicular to the film plane. Perpendicular anisotropy was found only in a narrow range of thickness ∼10 nm. These alloys exhibit magnetic compensation ∼175 K, where the 4.9 μ_B moment of the cobalt subnetwork measured in a-YCo_3 was practically con-

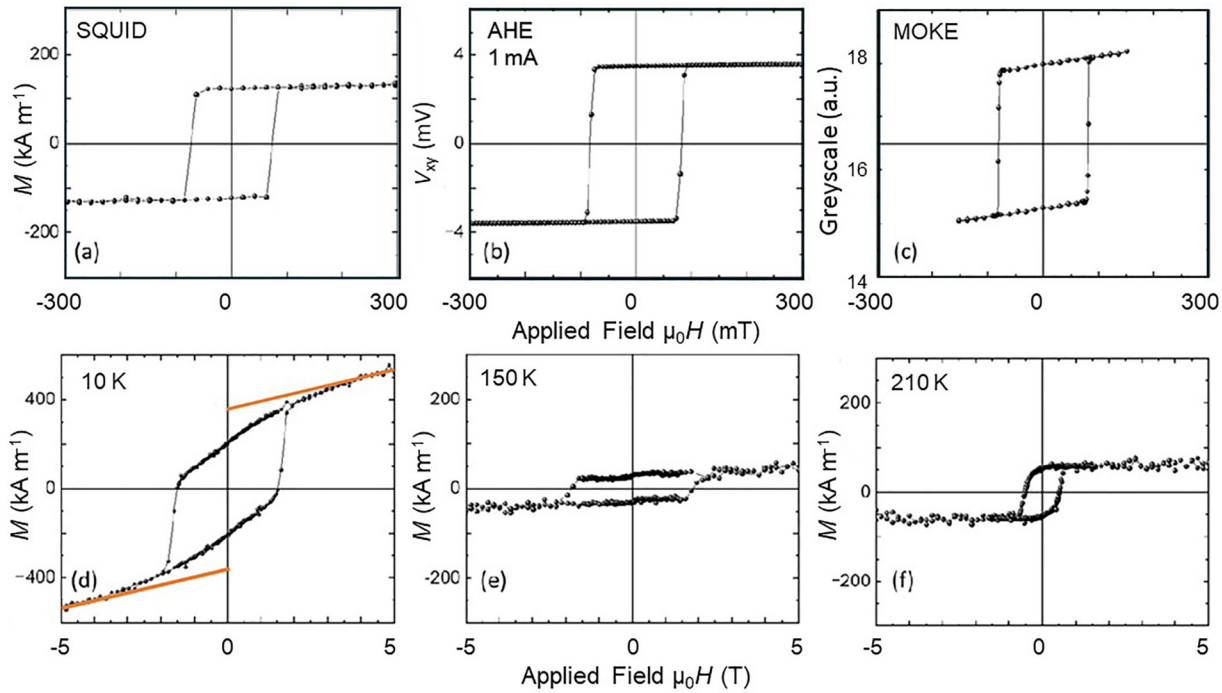

FIG. 2. Some representative hysteresis loops of a-$DyCo_3$. Top row: Measured at 300 K by (a) superconducting quantum interference device (SQUID) magnetometry perpendicular to the film plane, (b) anomalous Hall effect (AHE), and (c) magneto-optic Kerr effect (MOKE). Bottom row: Measured by SQUID magnetometry at (d) 10 K, (e) 150 K, and (f) 210 K.

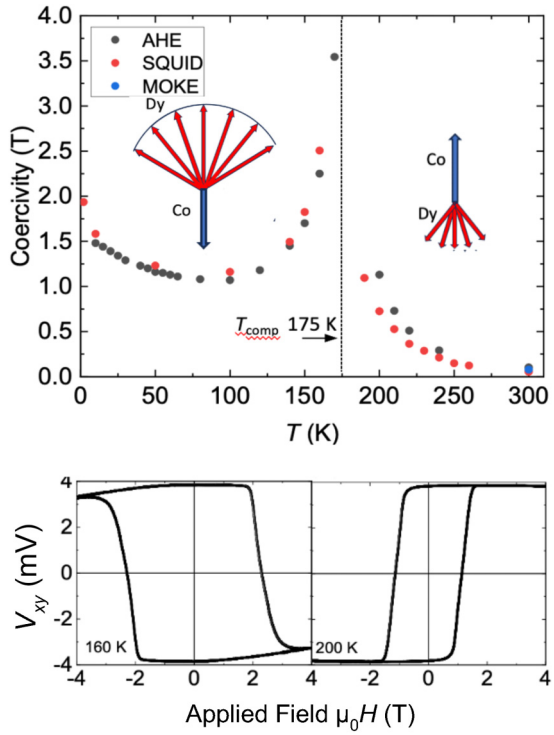

FIG. 3. Coercivity for a-$Dy_{0.25}Co_{0.75}$ showing divergence at the compensation temperature of 175 K. Data points are obtained by superconducting quantum interference device (SQUID) magnetometry or anomalous Hall effect (AHE). A magneto-optic Kerr effect (MOKE) point at 300 K is included. AHE loops taken below and above compensation are illustrated in the lower panels.

stant from 4 to 300 K on account of the high Curie temperature [18]. Hysteresis loops measured using different techniques are shown in Fig. 2. The plot in Fig. 3 of the coercivity taken from magnetization and anomalous Hall loops as a function of temperature illustrates the divergence at T_{comp}. Compensation is accompanied by reversal of the sign of the Hall loops. The AHE, like the Kerr effect in amorphous rare-earth cobalt alloys, arises more from the cobalt magnetization [32] rather than the rare-earth 5*d*/6*s* conduction electrons because the magnitude of the effect depends little on the alloyed rare-earth atom or temperature [33]. A recent report on the AHE in crystalline $GdCo_3$ and $GdCo_5$ intermetallics suggests that rare-earth and cobalt contributions of opposite signs reinforce each other in the crystalline ferrimagnetic structures [34].

The magnetic moment *m* in Bohr magnetons per a-$DyCo_3$ amorphous formula unit is plotted in Fig. 4, considering the sign change at compensation. The axis on the right indicates the net moment per dysprosium atom, if the contribution of the cobalt subnetwork remains constant at 4.9 μ_B; the net Dy moment must have this value at T_{comp}. There is an upturn in remanence <50 K, which is associated with a high-field linear term in magnetization up to saturation which appears only at low temperature in Fig. 2(d). The remanence and saturation curves diverge significantly when *K*, the net anisotropy of the film, is no longer sufficient to maintain the magnetization perpendicular to the film plane. The bulk anisotropy energy of the thin film was estimated as 20 kJ m^{-3} at 50 K from the maximum magnetization where the hysteresis loop remains

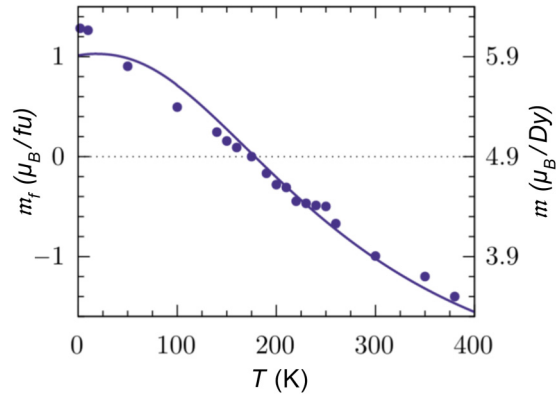

FIG. 4. Magnetic moment per $DyCo_3$ formula unit in a-$Dy_{0.25}Co_{0.75}$, considering the change of sign at T_{comp}. The average moment per dysprosium atom is marked on the right-hand scale. The solid line is a fit to the data based on Eq. (2) with negative B_2^0.

square (see also Sec. IV B) and a similar value 28 kJ m^{-3} was deduced from the 375 mT saturation field M_s in the hard-axis magnetization curve at 300 K using the relation $K = \frac{1}{2}B_a M_s$. The atomic moment per dysprosium atom in the alloy is 10.4 μ_B (10 μ_B from $J = \frac{15}{2}$ and a Landé g factor $g_L = \frac{4}{3}$ with an estimated contribution of 0.4μ_B from the 5*d*/6*s* electrons). The extrapolated moment is 7.2 μ_B/Dy, which corresponds to a cone half-angle of 65°.

A 10 nm $DyCo_3$ film that exhibited partial single-pulse all-optical switching [11] was selected for an x-ray photoemission electron microscopy (XPEEM) investigation on the UE49 PMGa SPEEM beamline at the BESSY II Synchrotron facility at Helmholtz-Zentrum Berlin. Details are given in Secs. IV E and S1 in the Supplemental Material [35].

B. Terbium alloys

The a-$Tb_{0.25}Co_{0.75}$ films studied were ∼20 nm thick and exhibited perpendicular anisotropy (Fig. 5). Most of them show a sharp increase of magnetization in their SQUID hysteresis loops close to remanence; there is an example in Fig. 5(d). Remarkably, there is never any trace of this soft phase in either Hall or Kerr hysteresis loops, which are shown for the same film at 300 K in Figs. 5(e) and 5(f). This is explained in Sec. S2 in the Supplemental Material [35].

A plot of the coercivity of a-$Tb_{0.25}Co_{0.75}$ as a function of temperature shown in Fig. S3 in the Supplemental Material [35] is very similar to that of a-$Dy_{0.25}Co_{0.75}$ in Fig. 3. It tends to diverge at the compensation temperature of ∼200 K, where a thermal scan of remanence crosses zero (Fig. 6). There is no pronounced appearance of a component with a high-field slope at low temperature, possibly because the Tb films have greater perpendicular anisotropy. The low-temperature saturation magnetization of the Tb atoms is 6.9 μ_B.

C. Thulium alloys

In-plane magnetization curves of the a-$Tm_{0.25}Co_{0.75}$ film are plotted in Fig. 7. Due to shape anisotropy, the magnetization is in-plane at 300 and 200 K, and it begins to rotate toward the perpendicular direction at 100 K. Interpolation

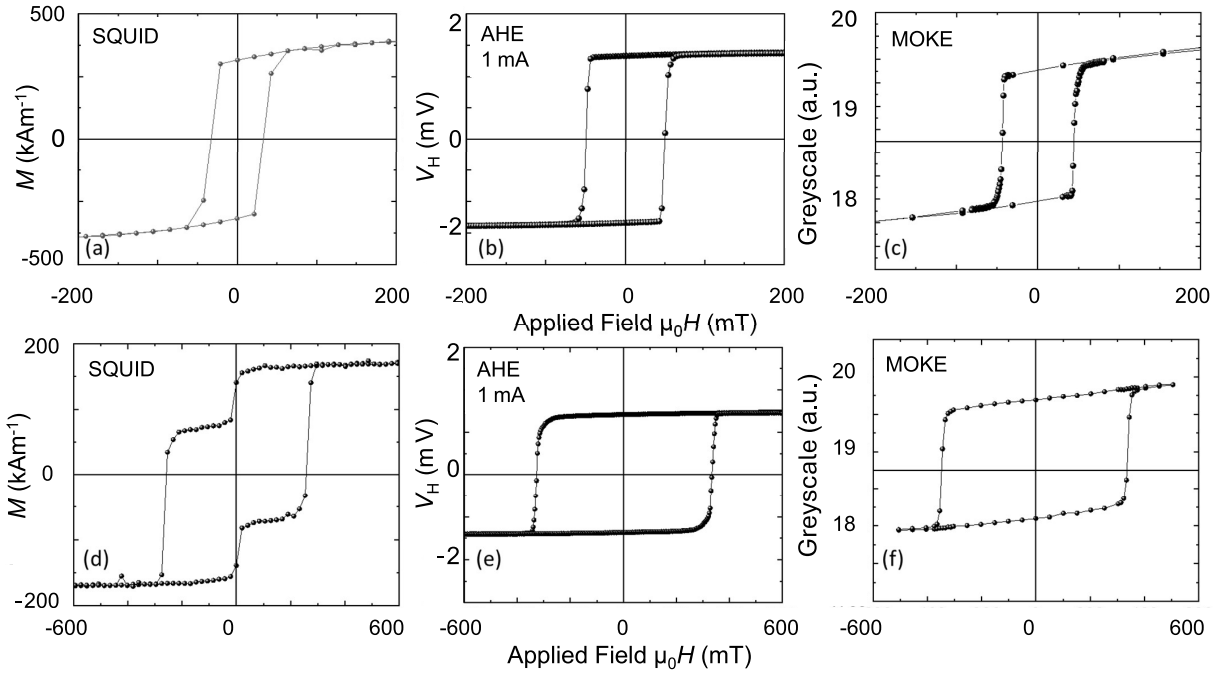

FIG. 5. Magnetization loops of a sample of a-$Tb_{0.21}Co_{0.79}$ (top row, film 6) and a-$Tb_{0.25}Co_{0.75}$ (bottom row, film 5) measured by superconducting quantum interference device (SQUID) magnetometry (left), anomalous Hall effect (center), and Kerr effect (right). The step at remanence is seen in some SQUID loops but never in the Hall or Kerr loops. All measurements are made at room temperature.

between 100 and 70 K indicates that the spin reorientation is complete at 85 K; the magnetization of 180 kA m^{-1} becomes perpendicular and remains so down to 5 K. Compensation is at 50 K, but coercivity never exceeds 0.5 T. The perpendicular anisotropy constant K deduced from the magnetization where the spontaneous spin reorientation occurs is $K = \frac{1}{2}\mu_0 M^2 = 23$ kJ m^{-3}. Above 100 K, shape anisotropy dominates, and the magnetization lies in-plane, as it does at all temperatures in a-Y_xCo_{1-x} [18].

The magnetization in Bohr magnetons per a-$TmCo_3$ formula unit is plotted in Fig. 8. The cobalt magnetization is taken from a-YCo_3 to be 4.9 μ_B and essentially constant below room temperature. The temperature dependence of the average Tm subnetwork moment is also indicated in the figure.

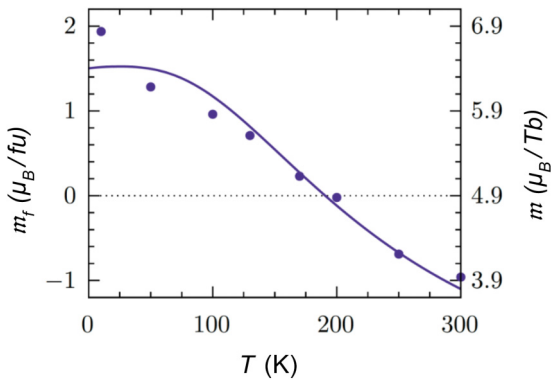

FIG. 6. Magnetic moment per $TbCo_3$ formula unit in a-$Tb_{0.25}Co_{0.75}$, considering the change of sign at T_{comp}. The average moment per Tb is shown on the right-hand scale. The solid line is a fit to the data based on Eq. (2) with negative B_2^0.

The low-temperature magnetization of Tm is 5.8 μ_B. The $4f$ magnetic moment of the Tm atom is 7.0 μ_B, giving $\langle J_z\rangle/J = 0.83$ at 5 K and $\theta_0 = 47°$.

IV. DISCUSSION

A. Random local electric fields

The product of the quadrupole moment of the $4f$ shell and the diagonal local electric field gradient that depends on the Stevens operator $\hat{\mathbf{O}}_2^0 = 3\hat{\mathbf{J}}_z^2 - J(J+1)$ is just 5% greater for

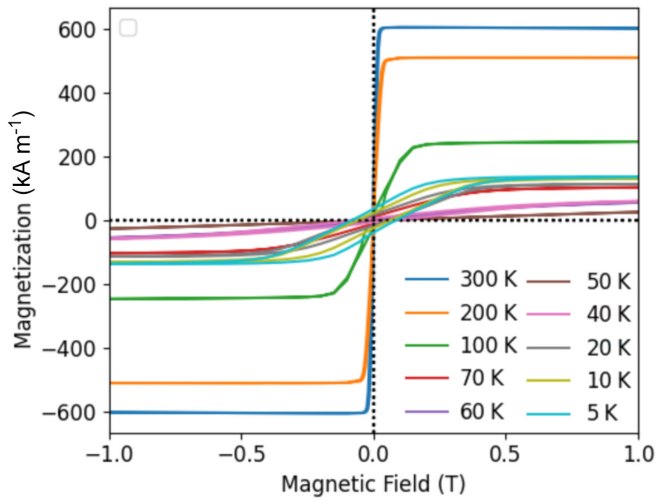

FIG. 7. Magnetization curves of a-$Tm_{0.25}Co_{0.75}$ with field applied in-plane. The anisotropy is perpendicular to the film plane <85 K. Compensation is at 50 K.

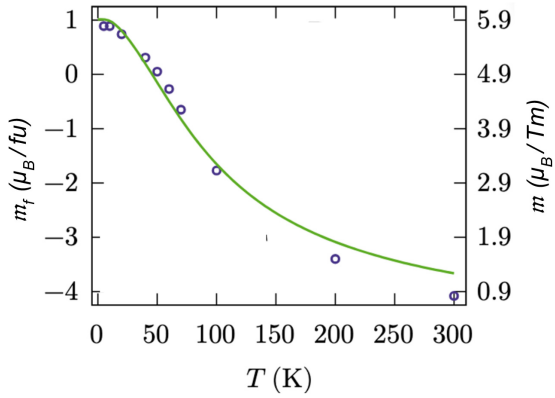

FIG. 8. Magnetization of a-$Tm_{0.25}Co_{0.75}$ vs temperature. The solid line is a fit of Eq. (2) with positive B_2^0 to the data.

Tb ($J = 6$) than for Dy ($J = \frac{15}{2}$) at $T = 0$ [30], so the leading second-order term in the local random anisotropy energy is similar for the two elements. Dy and Tb have random easy axes distributed over a sphere. The Tm quadrupole moment and the second-order anisotropy energy have opposite signs, but the magnitude of the anisotropy is similar for Tb, Dy, and Tm. See Table S1 in the Supplemental Material [35].

The difference between the two signs of anisotropy is illustrated in Fig. 9. Weak antiferromagnetic exchange with Co will select directions for easy-axis anisotropy lying in the hemisphere around the z direction, opposite to the Co axis so that the average reduced moment $\langle J_z\rangle/J = (\cos\theta)_{\rm av} = \frac{1}{2}$, where $(\,)_{\rm av}$ denotes the geometric average over a hemisphere. Tm is different. The random anisotropy axes are now hard axes, and equivalent easy directions lie in a circle perpendicular to the axis. Weak antiferromagnetic exchange with Co now selects an easy direction in the yz plane as shown in the figure and $\langle J_z\rangle/J = (\sin\theta)_{\rm av} = \pi/4 = 0.785$. Increasing exchange with Co will narrow the distributions of directions in the hemisphere and increase $\langle J_z\rangle/J$ in either case. The resulting sperimagnetic rare-earth distributions are modeled by uniform distribution of orientations within a cone of half-angle θ_0 that gives the correct net rare-earth moment. Note that random hard axes give a larger net moment than random easy axes.

However, when the random axes are hard, it is insufficient to consider only the diagonal second-order term. The general second-order energy surface is not an ellipsoid of revolution with equivalent directions perpendicular to the hard axis but a general ellipsoid with three principal axes that depend on the off-diagonal Stevens operator $\hat{\mathbf{O}}_2^2 = \frac{1}{2}(\hat{\mathbf{J}}_+^2 + \hat{\mathbf{J}}_-^2)$. The energy

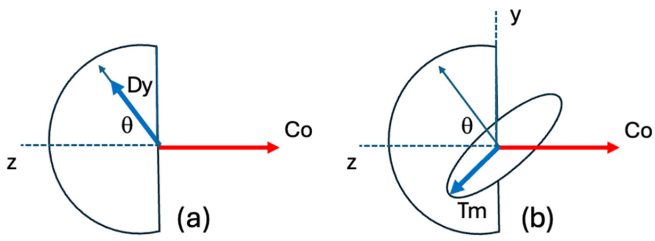

FIG. 9. Random anisotropy in a hemisphere (a) easy axis and (b) hard axis.

surface in the plane is no longer a circle but an ellipse, and the easy axis no longer lies in the yz plane. The z projection of the moment in the weak exchange field from cobalt is therefore less than $\pi/4$.

Terms of fourth and sixth order in the local crystal field theory represent the interactions of the 16-fold (hexadecapole) and 64-fold moments of the $4f$ electronic charge distributions with the appropriate local electric field gradients. The diagonal Stevens operators include terms that vary as $\hat{\mathbf{J}}_z^4$ and $\hat{\mathbf{J}}_z^6$, respectively, whose influence falls off rapidly with increasing temperature, but there are also terms in lower even powers of $\hat{\mathbf{J}}_z^2$ that contribute to the uniaxial anisotropy. The higher-order terms that influence the variation of the rare-earth magnetism at low temperature are opposite in sign to the second-order anisotropy for Tb (fourth order) and Dy (sixth order) [30]. Details are included in Sec. S3 in the Supplemental Material [35].

The J values for Dy, Tb, and Tm are 7.5, 6, and 6, respectively, and the magnetic moments m of the $4f$ shells are 10 μ_B, 9 μ_B, and 7 μ_B. Gd, by contrast, has no $4f$ quadrupole moment, and it is insensitive to local electrostatic fields; its $4f$ magnetic moment of 7 μ_B has purely spin character. The a-Gd_xCo_{1-x} alloys are ferrimagnets, whereas the amorphous alloys a-R_xCo_{1-x} with Tb, Dy, or Tm are sperimagnets. All four exhibit compensation near or below room temperature when $x \approx 0.25$. Their $4f$ spin angular momenta in units of $\hbar$ are 3.5, 3, 2.5, and 1, respectively, so the R-Co exchange energy is expected to decrease in this sequence. The a-Y_xCo_{1-x} alloys are ferromagnets, provided any $4d$ moment on yttrium can be neglected (Fig. 1). Those alloys are very soft, with a coercivity of order 1 mT at 300 K [18].

B. Sperimagnetism

1. Tb and Dy

It is clear from Figs. 4 and 6 that the amorphous Tb and Dy alloys are not collinear ferrimagnets, at least in their ground state. If they were, the measured moments at low temperature would be 4.1 μ_B and 5.1 μ_B, respectively, assuming the same collinear cobalt moment of 4.9 μ_B, as measured for a-YCo_3 by magnetization and XMCD [18] and ignoring any contribution to the rare-earth moment from the $5d$ conduction electrons. (If a $5d$ contribution of 0.5 μ_B and 0.4 μ_B, respectively, is included, the expected values are 4.6 μ_B and 5.5 μ_B.) The measured values of 1.2 μ_B and 2.0 μ_B at low temperature are notably smaller. Our extrapolated Dy moment of 7.5 μ_B [Fig. 2(d)] is consistent with literature values that range from 6.7 μ_B to 8.5 μ_B, depending on the choice of moment for Co and the precise composition and preparation procedure [15,17,19,20,22].

The cobalt subnetwork is strongly ferromagnetic and insensitive to local atomic-scale random anisotropy at the cobalt sites because of the exchange averaging [18]. The Curie temperature of a-YCo_3 is $T_C \approx 760$ K [28,29], and the corresponding molecular field coefficient $n_{Co-Co} = T_c/C$, where $C = \mu_0 n g^2 \mu_B^2 S(S+1)/3k_B$ is the Curie constant. The Weiss molecular field $H_W^{Co\text{-}Co} = n_{Co\text{-}Co}M$, where the magnetization $M = ng\mu_B S$ and n is the number of Co atoms per m^3 [30]. It follows that the exchange field depends on T_C, the effective

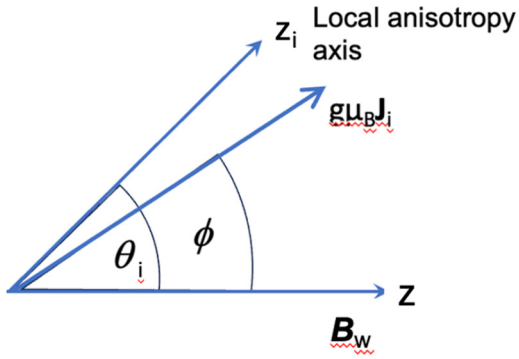

FIG. 10. Classical picture of the magnetic moment of a rare-earth atom at site i in an amorphous rare-earth cobalt alloy subject to a molecular field $\mathbf{B}_w$ from the cobalt along the $-z$ axis and uniaxial anisotropy directed along a local axis $\mathbf{z}_i$ making an angle θ_i with the z axis.

spin quantum number and the g factor of cobalt

$$\mu_0 H_{\rm ex}^{\rm Co\text{-}Co} = \frac{3k_{\rm B}T_{\rm C}}{g(S+1)\mu_{\rm B}}. \tag{1}$$

The exchange field $\mu_0 H_{\rm ex}^{\rm Co\text{-}Co}$ acting on the ferromagnetic cobalt is 855 T, assuming $S = 1$ and $g = 2$. The exchange energy is 1137 K/Co atom, and the ratio α of anisotropy to exchange energy is 0.005 [18].

The reduction in rare-earth moment of Tb and Dy is attributed to a much greater ratio of random anisotropy energy to exchange energy than in Co. In amorphous a-Gd_xCo_{1-x}, where there is no random anisotropy, the low-temperature moment of a-$Gd_{0.22}Co_{0.78}$ of 2.0 μ_B per formula unit [36] corresponds to the full metallic moment of 7.6 μ_B per Gd, taking the cobalt moment as 1.6 μ_B. To analyze the noncollinearity of Dy and Tb, we need to know the magnitude of the random anisotropy and the magnitude of the R-Co exchange energy acting on the rare earth.

The local anisotropy energy rare-earth atom in a magnetically ordered a-R_xCo_{1-x} alloy with second-order uniaxial local anisotropy of uniform magnitude that is not a small perturbation on the exchange is properly described by the one-atom Hamiltonian

$$\mathcal{H}_i = 3B_2^0\left[\left(\hat{\mathbf{J}}_z\cos\theta_i + \hat{\mathbf{J}}_x\sin\theta_i\right)^2 - \left(\tfrac{1}{3}\right)\hat{\mathbf{J}}^2\right] - g_s\mu_{\rm B}\hat{\mathbf{J}}_z B_{\rm ex}^{R\text{-Co}}. \tag{2}$$

The first term in Eq. (2) is the axial second-order crystal-field energy, where the parameter B_2^0 combines information on the quadrupole moment of the rare-earth atom and the local electric field gradient that will depend on the composition x. The second term is the Zeeman energy in the exchange field approximation where $g_s = 2S/J$ is the spin g factor for the heavy rare earth since the exchange interaction couples Co and rare-earth spins. In the Weiss molecular field theory, we would use the Landé g factor and replace $B_{\rm ex}$ by $B_{\rm W}$. Here, θ_i is the angle between the magnetization axis of the cobalt subnetwork and the local uniaxial symmetry axis $\mathbf{z}_i$ that is different at every rare-earth site. The vector model of Fig. 10 is the classical representation of the model of Eq. (2).

The complete description of the second-order crystal field of a rare-earth atom includes another off-diagonal energy term $B_2^2\hat{\mathbf{O}}_2^2$ in the Hamiltonian describing the asymmetry of the energy in the plane perpendicular to the local easy axis, which now depends on two angles and involves all three operators $\hat{\mathbf{J}}_x$, $\hat{\mathbf{J}}_y$, and $\hat{\mathbf{J}}_z$ [37,38]. The local second-order energy surface is a general ellipsoid with three principal axes, one easy and two hard, or vice versa.

An approximation valid in the limit when α, the ratio of anisotropy to exchange energies $3B_2^0/g_s\mu_{\rm B}JB_{\rm ex}^{R\text{-Co}}$, is $\ll 1$ replaces the first term in Eq. (2) by $D\hat{\mathbf{J}}_{zi}^2$ with $D = 3B_2^0$ instead of $B_2^0(3\hat{\mathbf{J}}_{zi}^2 - \hat{\mathbf{J}}^2)$; the term in brackets is $\hat{\mathbf{O}}_2^0$, the Stevens operator equivalent for the diagonal term in the electrostatic quadrupole interaction referred to the local easy axis. This small-α approximation is the Harris, Plischke, Zuckerman model [39], but the $\hat{\mathbf{J}}^2$ term with diagonal elements $J(J+1)$ is needed to ensure that the anisotropy vanishes at high temperatures when all the M_{Ji} states of a particular single ion are equally populated. It is equivalent to representing the leading term in the bulk magnetocrystalline anisotropy by $K_1\sin^2(\theta-\phi)$. The local anisotropy is exchange-averaged by the exchange field when $\alpha \ll 1$, as in a-Y_xCo_{1-x}, but when $\alpha \gtrsim 1$, the local magnetization direction approaches $\mathbf{z}_i$ and $(\theta_i - \phi)$ becomes small; the small-α approximation is no longer valid because $\sin^2(\theta_i - \phi)$ is then always less than $\cos\theta_i$.

We assume further that both $\boldsymbol{B}_{\rm ex}$ and B_2^0 have the same magnitude at every site and are independent of temperature. The assumption for $\boldsymbol{B}_{\rm ex}$ is justified by the high T_C of a-YCo_3 and previous measurements on this alloy [18]. Values of $B_{\rm ex}$ and $B_2^0 = D/3$ are then needed to define α. The anisotropy parameter has been estimated experimentally for several systems of rare-earth rich amorphous R-X alloys, where R = Tb or Dy and X = Cu, Ag, or Au, which exhibit spin freezing at temperatures in the range 20–70 K [40]. For example, a value of D = 3 K was deduced from the large linear low-temperature specific heat of a-$Dy_{0.41}Cu_{0.59}$ [41]. Similar estimates of D were based on the approach to saturation of a-$R_{0.50}Ag_{0.50}$ alloys [42,43]. The electric field gradient at the rare-earth site in transition-metal-rich a-$R_{0.25}T_{0.75}$ alloys should be greater than it is in a-RX because of the shorter average nearest-neighbor distances. Estimates may be obtained from a-$R_{0.25}Ni_{0.75}$ [43,44], where the Ni is nonmagnetic but similar in size to Co. Random spin freezing then occurs as a result of weak R-R exchange and random anisotropy at 10 K for R = Dy. This indicates that R-R exchange can be neglected in our system. A fit of the linear magnetization curve at 1.4 K in high fields from 8 to 15 T, where the moment per Dy is ~6 μ_B gave D = 5.8 K [44]. The corresponding spin-freezing temperature and D for Tb would be 12 and 6.1 K, scaling by the rare-earth spin and quadrupole moments, respectively [30]. Substantially larger values of D have been reported in sperimagnets where the rare earth is simultaneously subject to random anisotropy and a large molecular field from cobalt [37,45,46].

In Fig. 11, we show a plot of the zero-temperature reduced magnetization $\langle J_z\rangle/J$ vs α over the range $0 < \alpha < 6$, calculated from Eq. (2), where $\langle J_z\rangle/J = \langle m\rangle/m_0$ is evaluated for different values of α by diagonalizing the one-atom Hamiltonian of Eq. (2) and averaging over the axes in a hemisphere. The plots for $J = \frac{15}{2}$ (Dy) and $J = 6$ (Tb) are very similar.

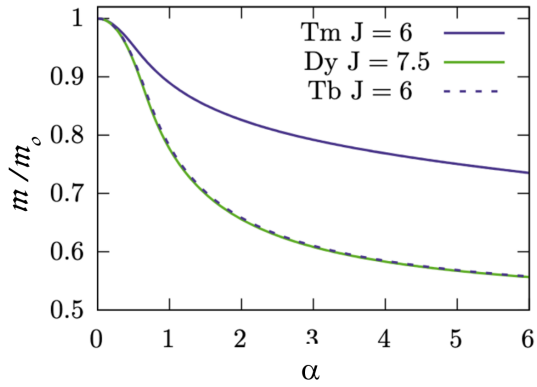

FIG. 11. Reduced low-temperature magnetization $\langle m\rangle/m_0$ calculated from Eq. (2) for $J = \frac{15}{2}$ Dy or $J = 6$ Tb atoms with random easy-axis anisotropy as a function of α and for $J = 6$ Tm atoms with random hard-axis anisotropy as a function of $-\alpha$, the ratio of anisotropy to exchange energy per atom.

When $\alpha \ll 1$, we find the classic approach to saturation for randomly oriented uniaxial particles varying approximately as $1/B^2$, which was recently reevaluated by Zhang *et al.* [47]. The exchange energy a-$GdCo_{3.55}$, where there is no random anisotropy can be deduced from the compensation temperature, which is 315 K [36]. The exchange field B_{ex} required to induce a magnetization of 5.68 μ_B, the Co moment at this temperature [18], is 145 T for a Brillouin function $\mathcal{B}_{7/2}(x)$ with $g = 2$ (Sec. S3 in the Supplemental Material [35]). For the other heavy rare earths, the random anisotropy prevents the exchange field from aligning the moments along **z**, so the corresponding magnetic energy is less than that expected for the moment calculated from the Brillouin function. Based on the fits of the theory of Eq. (2) to the values of $\langle J_z\rangle/J$ near and above compensation in Figs. 4, 6, and 8, the values of B_{ex}, B_2^0, and α listed in Table S2 in the Supplemental Material [35] are obtained.

The difference between B_2^0 for Tb (-1.4 K) and Dy (-3.5 K) is surprising. The electric field gradient A_2^0 should be the same in each case because the structure of the a-$R_{0.25}Co_{0.75}$ alloys hardly depends on the rare earth. Since $B_2^0 = \theta_2\langle r^2\rangle A_2^0$, where θ_2 is the quadrupole moment and $\langle r^2\rangle$ is the mean square rare-earth radius, the electrostatic quadrupole interaction at low temperature will vary as $\theta_2\langle r^2\rangle[3J^2 - J(J+1)]$ for alloys of different rare earths with the same structure. This quantity is almost the same for Tb and Dy (Table S1 in the Supplemental Material [35]), so why are the B_2^0 values so different? The likely explanation lies in the higher-order axial crystal field terms. The operator $\hat{\mathbf{O}}_4^0$ contains terms in $\hat{\mathbf{J}}_z^4$, which become significant only at low temperatures, but also terms in $\hat{\mathbf{J}}_z^2$ that add to or subtract from α deduced from the fits. The signs of $\theta_2\langle r^2\rangle\ O_2^0(0)$ and $\theta_4\langle r^4\rangle\ O_4^0(0)$ are the same for Dy and opposite for Tb; the different values of α from the fits are reconciled if $B_2^0 = 3.9$ K and $B_4^0 = 1.5 \times 10^{-3}$ K.

However, the temperature dependence of the rare-earth moment calculated from Eq. (2), which has zero slope at $T = 0$ as expected, deviates obviously from the experimental remanence data for Dy and Tb $<\sim$50 K. The fits give moments $\langle m(0)\rangle$ of 5.9 μ_B and 6.4 μ_B for Dy and Tb, respectively, with corresponding cone angles θ_0 of 80° and 67°, but the measured or extrapolated magnetizations near $T = 0$ are greater, and the sperimagnetic cone angles are smaller. These low-temperature values are 7.5 μ_B and 60° for Dy and 6.9 μ_B and 59° for Tb.

The model of Eq. (2), based on a uniaxially symmetric local crystal field parameterized by a single constant B_2^0 or an equation with two constants B_2^0 and B_4^0 is oversimplified and underestimates the low-temperature moments significantly. The other second-order parameter B_2^2 reflects the asymmetry of the crystal field energy in the plane perpendicular to the local hard axis, while the fourth- and sixth-order terms reflect components with cubic or hexagonal symmetry. Higher-order diagonal terms with opposite signs to the second-order term make the local energy surface more spherical and reduce the energy for thermal excitation. The importance of the higher-order terms at low temperature is recognized in crystalline rare-earth metals and intermetallics such as $Nd_2Fe_{14}B$ [3], which becomes noncollinear with fourfold magnetic symmetry <135 K, and $SmCo_5$, where the sixth-order term contributes to the uniaxial anisotropy at low temperature [48]. Unlike a-YCo, where the random anisotropy is exchange-averaged because $\alpha \ll 1$, both a-$DyCo_3$ and a-$TbCo_3$ are in a strong pinning region $\alpha \geqslant 1$, where the local anisotropy is not a small perturbation but is comparable with the exchange. The coercivity of several Tesla at low temperature in these amorphous magnets is the result.

On increasing temperature toward compensation, the magnitude of the rare-earth moment is reduced by thermal excitation of excited M_J states, but the anisotropy is simultaneously weakened, and it falls off more rapidly with temperature than the magnetization, thereby narrowing the cone. We can calculate this effect for Dy in a-$DyCo_3$ using the data in Fig. 4 and the fit to Eq (2). If we assume that the thermal average of the magnitude of the Dy moment $\langle m(T)\rangle_{th}$ follows a $\mathcal{B}_{15/2}$ Brillouin function in the exchange field from Co, scaled by the Co magnetization calculated from $S = 1$ molecular field theory (the case with no random anisotropy and a ferrimagnetic structure), the values are 7.5 μ_B, 6.2 μ_B, and 5.1 μ_B at 200, 300, and 400 K, respectively. The measured values are 5.3 μ_B, 3.8 μ_B, and 3.0 μ_B. The cone angle has been reduced from 80° at 200 K to 65° at 400 K. The sperimagnetic structure may approach collinear ferrimagnetism close to T_C, but it persists well above room temperature in a-$DyCo_3$. In a-$TbCo_3$, however, there is little difference between the 300 K moment of 3.9 μ_B and 3.5 μ_B that would be induced by the fitted exchange field of 77 T on the $J = 6$ Tb atom; the sperimagnetism there is a low-temperature phenomenon, with Tb noncollinearity becoming important only below room temperature. The temperature sequence of the magnetic structure as a function of temperature in an a-$DyCo_3$ film with perpendicular magnetic anisotropy is illustrated schematically in Fig. 12.

2. Tm

A plot of the magnetization of a-$Tm_{25}Co_{75}$ as a function of temperature was shown in Fig. 8. The magnetization is essentially constant <20 K. The average low-temperature moment of Tm there is 830 kA m^{-1} or 5.8 μ_B along **z**, whereas the magnetic moment of the Tm atom is 7.0 μ_B, giving $\langle J_z/J\rangle = 0.83$

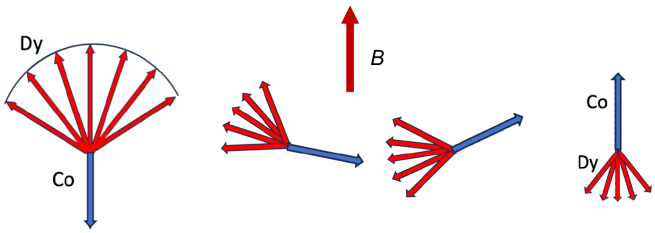

FIG. 12. Sequence of magnetic structures found with increasing temperature in a-$DyCo_3$ on passing through compensation in a field greater than the spin-flop field.

at $T \approx 0$ and a rather narrow cone angle $\theta_0 = 50°$. The fit values are 0.84 and 47°.

An important point here concerns coercivity, which is related to difficult-to-surmount barriers between moment-reversed micromagnetic states. It is governed by the rare earth because, as we have emphasized, random anisotropy in the cobalt subnetwork is exchange-averaged to zero. Reversal of a rare-earth moment with easy-axis anisotropy involves overcoming a barrier where the moment is perpendicular to the easy axis. There is no such barrier in a hard-axis system where all directions in the plane perpendicular to the hard axis are equally easy. The contrast between the Tm and Dy or Tb thin films is striking, particularly around compensation (Figs. 3, 7, and S3 [35]). The small residual coercivity for Tm at low temperature may be related to surface states since it is smaller in thicker films. An asymmetry of the second-order interaction is introduced by the off-diagonal second-order term in the crystal field $\mathbf{O}_2^2$, which selects a preferred direction within the easy plane, so the system has a distribution of weakly preferred easy axes at low temperature [38], with low-energy barriers that create little coercivity.

We have calculated the reduced moment vs the ratio $-\alpha$ of random anisotropy to exchange for Tm, $J = 6$, which was compared with the one for positive α for Tb, $J = 6$, in Fig. 11. The fit to the data in Fig. 8 is poor at room temperature, but it is improved by increasing the magnitude of B_2^0 to a value closer to those for Dy and Tb.

C. Perpendicular magnetic anisotropy

The magnitude of the intrinsic perpendicular anisotropy in the a-$DyCo_3$ and a-$TbCo_3$ films [$\gtrsim$20 kJ m^{-3}, including the room-temperature estimate of 28 kJ m^{-3} from the linear in-plane magnetization of film 2 in Fig. 2(a)] is smaller than that inferred from the perpendicular magnetization curves of a-Y_xCo_{1-x} (46 kJ m^3), where the large net magnetization lies in-plane [18]. This suggests that cobalt rather than the rare earth may be the principal source of perpendicular anisotropy in the Dy and Tb films. Several possible origins of the anisotropy have been discussed in the past, but it is difficult to disentangle them in any particular case. They include surface contributions from the upper and lower surfaces of the thin film, a bulk term associated with substrate-induced strain during deposition, and a structural term due to alignment of *R*-T pairs at the surface [49], *R*-Co pairs perpendicular to the film surface [50], or oxygen in the structure [51]. Furthermore, the local easy axes of rare-earth atoms at the surface or interface will no longer be random and isotropic. Nanoscale inhomogeneity in the form of columnar rare-earth clusters has been demonstrated for a-Gd_xFe_{1-x}, and the degree of atomic order or clustering varies with film thickness [52]. A straightforward empirical separation of bulk and surface contributions based on their scaling with film volume and area is obtained from a plot of $tK_{\rm eff}$ vs t, where $K_{\rm eff}$ is the total effective anisotropy and t is the film thickness. This gives the bulk and surface contributions from the slope and y-axis intercept, respectively. Applied to a-$Tb_{0.12}Co_{0.88}$, the method showed that the surface contribution favors an easy plane and the bulk term an easy axis, with a crossover $<$10 nm [32], like our a-$Dy_{0.25}Co_{0.75}$. However, the bulk term changes sign in response to some change of composition [42] or amorphous atomic structure with film thickness, which is best approached by a systematic empirical exploration of the effect of growth parameters, such as was carried out for a-GdFeCo by Hansen *et al.* [7]. Perpendicular anisotropy in the Tm system was discussed in Sec. III C. In all three cases, the anisotropy is perpendicular when the magnetization is $<$250 kA m^{-1}. The anisotropy becomes in-plane for larger magnetization because of the shape anisotropy of a thin film.

D. Compensation

The behaviors of a crystalline anisotropic antiferromagnet and a crystalline anisotropic ferrimagnet at compensation are similar; two rigid sublattices, A and B, are coupled by intersublattice exchange, represented in molecular field theory by a Weiss field $H_{\rm W} = n_{\rm AB}M_\alpha$, where M_α, α = A, B, are sublattice magnetizations and $n_{\rm AB}$ is the intersublattice molecular field coefficient. The compensated ferrimagnet behaves like an antiferromagnet in a field applied parallel to the antiferromagnetic axis (Néel vector) defined by the anisotropy field $H_{\rm a} = K/\mu_0 M_\alpha$, and both undergo a spin-flop transition to a canted configuration in a critical field $H_{\rm sf}$ given by [30]

$$H_{\rm sf} = 2\sqrt{(H_{\rm a}H_{\rm W})} \tag{4}$$

that is valid provided $T_{\rm sf}$ is much less than the Néel temperature $T_{\rm N}$ since the parallel susceptibility $\chi_{||}$ can then be neglected compared with $\chi_\perp = M_\alpha/H_{\rm W} = -1/n_{\rm AB}$. The net magnetization in a field H applied perpendicular to the antiferromagnetic axis is $2M_\alpha H/H_{\rm W}$. By convention, $n_{\rm AB}$ is negative, and the vectors $\boldsymbol{M}_{\rm A}$ and $\boldsymbol{M}_{\rm B}$ are of opposite sign. Spin flops are observed in antiferromagnets over a wide range of temperatures since $M_A = M_{\rm B}$. It is also possible to flop the magnetization of a ferrimagnet in a narrow range of temperature on either side of compensation where $M_A \neq M_{\rm B}$ in a field greater than $H_{\rm sf}$, provided the net magnetization is small. Ferromagnetic saturation requires a much larger applied field, of order $H_{\rm W}$.

Crystalline [53,54] and amorphous ferrimagnets such as a-Gd_xCo_{1-x} and a-$Gd_x(Fe,\ Co)_{1-x}$ [7,34,55–57] flop similarly in fields applied parallel to the anisotropy axis (anisotropy is essential; otherwise, the antiferromagnetic axis would fluctuate spontaneously). Written in terms of the anisotropy constant K, Eq. (4) becomes

$$H_{\rm sf} = 2\sqrt{\left(\frac{K}{\mu_0\chi_\perp}\right)}. \tag{5}$$

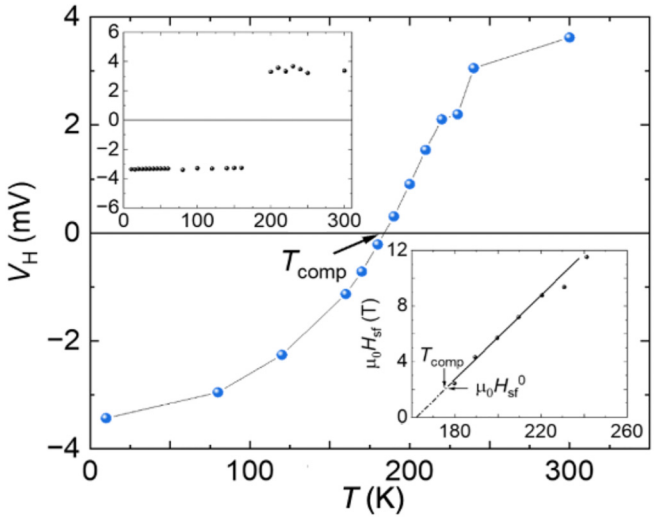

FIG. 13. Anomalous Hall voltage for a-$DyCo_3$ at saturation in 14 T measured with a current of 1 mA. Insets show the temperature dependence of the spin-flop field >175 K and the temperature dependence of the anomalous Hall voltage.

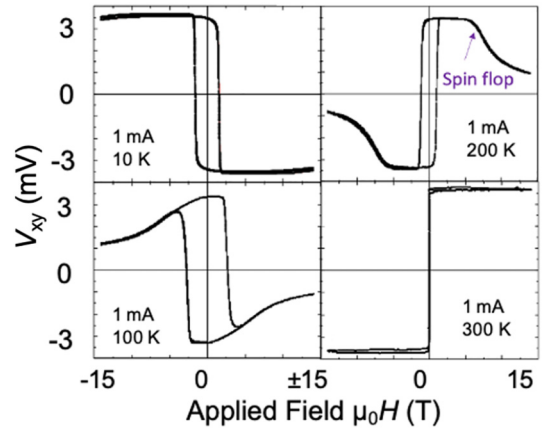

FIG. 14. Examples of the 14 T Hall loops measured above and below $T_{comp} = 175$ K. The decreases in high fields above and below T_{comp} are due to incipient spin flops.

Equation (5) emphasizes that the spin flop depends on essentially two physical quantities: the bulk anisotropy and the susceptibility perpendicular to the antiferromagnetic axis.

Sperimagnets at compensation differ from antiferromagnets or ferrimagnets at compensation. The rare-earth subnetwork is not rigid, and its resultant magnetization does not respond like a single vector. It is a frustrated system with local anisotropy competing with the exchange field from cobalt. The initial perpendicular susceptibility will be much greater than the value $-1/n_{AB} \approx 0.01$ expected in a system of two rigid sublattices.

Figure 13 shows measurements of the AHE of sperimagnetic a-$DyCo_3$ in fields of 14 T over the temperature range from 10 to 300 K. Unlike an antiferromagnet, where there is a well-defined spin flop in a field H_{sf} that increases with decreasing temperature, a ferrimagnet or sperimagnet shows a spin flop at T_{comp} in a field H_{sf}^0 and incipient spin flops that begin at H_{sf}^0 and increase linearly with $|T - T_{comp}|$; the net moment close to compensation is proportional to $|T - T_{comp}|$. In Fig. 14, the incipient spin flop for the cobalt subnetwork at 200 K is indicated by the purple arrow. A plot of H_{sf} vs temperature in an inset to Fig. 13 extrapolates to $\mu_0 H_{sf}^0 = 2.0$ T at $T_{comp} = 175$ K. The slope M vs $|H_{sf} - H_{sf}^0|$ is 9×10^{-3}. We can estimate H_{sf}^0 from Eq. (4) if we know H_W and H_a. Taking $K_1 = 22\,\mathrm{kJ\,m^{-3}}$ and $M_\alpha = 700\,\mathrm{kAm^{-1}}$, $H_a = K/\mu_0 M_\alpha \approx 10^5\,\mathrm{Am^{-1}}$. The exchange field acting on the cobalt subnetwork is 98 T (Table S2 in the Supplemental Material [35]) or 78 $\mathrm{MA\,m^{-1}}$; hence, the estimated value of μH_{sf}^0 is 7 T, notably more than the extrapolated value, as discussed above; a spin-flop field of 2.0 T requires $\chi_\perp \approx 0.1$. The susceptibility at compensation for Tm (Fig. 7) is likewise much greater than expected from the value of the exchange field $B_{ex} = 104$ T.

A feature if the hysteresis loops in Fig. 14 is that the deviation from saturation of the cobalt magnetization measured by AHE sets in close to zero field below compensation and at higher field above compensation. This is unlike a-Gd(Fe,Co), where the deviation from saturation is symmetric below and above T_{comp} [56], see Sec. S5 in the Supplemental Material [35]. In a sperimagnet, the asymmetry reflects the dominant magnetic subnetwork. It is Dy below and Co above compensation. Whereas the magnitude of the Co subnetwork moment is insensitive to applied field in this temperature range, the cone angle of the Dy will be reduced with increasing temperature; the effect of an applied field of 5 T will be to increase or decrease the Dy average moment by ∼5% below or above compensation, respectively. There is little evidence of any temperature-dependent 5*d*/6s Dy contribution to the AHE below compensation in the top inset to Fig. 13 [33].

The spin flop at compensation was illustrated schematically in Fig. 12. Above compensation, the magnitude of the Co subnetwork is dominant, and both the Dy moment and the random anisotropy are reduced with increasing temperature, leading to a smaller cone angle θ_0 and a more collinear sperimagnetic structure, which will have become ferrimagnetic near the Curie temperature.

E. Sperimagnetic domains and all-optical switching

Our study of partial single-pulse all-optical toggle switching by XPEEM in a-$DyCo_3$ confirms that the effect is observed both above and below the compensation temperature, but the laser power required to switch the domain structure increases in the same way with decreasing temperature as the local anisotropy energy. It is the magnitude of the local rare-earth anisotropy that controls the switch, not the macroscopic magnetization or the anisotropy field.

The point of interest in the context of magnetism of sperimagnetic a-$DyCo_3$ is the domain size in the demagnetized state. The domains are not fixed regions of the film that switch, but they appear in different positions every time. Switching seems to be uncorrelated with defects or spatial inhomogeneity in the film. The domain size lies mostly ∼200 nm at 300 K (Fig. S1 in the Supplemental Material [35]) and changes little down to 29 K. The model of three-dimensional wandering-axis ferromagnetism applied to a-YCo_3, where the domain size varies as $1/\alpha^2$ [18], predicts domains two orders of magnitude smaller than those we observe. The 10 nm film really

is a two-dimensional micromagnetic system, and the behavior appears to be related to the perpendicular magnetic anisotropy, which also varies little with temperature. In this respect, the sperimagnetic domains are akin to the maze domains found in ferromagnetic thin films, which are also related to perpendicular magnetic anisotropy [21].

It is interesting that complete single-pulse all-optical toggle switching is a purely thermal effect that has only been found in films of ferrimagnetic a-*R*T alloys containing Gd [58] or Mn-based films of crystalline ferrimagnetic metals [59]. The common feature is an element (Gd, Mn) with an atomic configuration corresponding to a stable half-filled shell, $4f^7$ or $3d^5$, having a first excited multiplet at an energy greater than that of the laser pulse. Hund's third rule is respected in the excitation process.

V. CONCLUSIONS

It is a formidably complex challenge to provide a complete account of the random crystal field acting on the magnetism of the rare earth in these amorphous alloys. There are up to 11 crystal field parameters, each with a distribution of magnitude. Even with complete magnetic data on isostructural alloys of all eight trivalent rare-earth atoms with an orbital moment, the experimental problem is underdetermined. The progress here depended on a comparison of three elements with similar magnitudes but different signs of the electric quadrupole and hexadecapole interactions, in different ranges of temperature.

Most striking perhaps is the tighter sperimagnetic cone angle and the absence of any large divergent coercivity at compensation in the hard random-axis Tm case, unlike the soft random-axis Tb and Dy cases. Also noteworthy is the low value of the Dy spin-flop field at compensation, associated with the large transverse susceptibility of the non-rigid sperimagnetic subnetwork.

The extrapolated rare-earth contribution to the low-temperature magnetization of amorphous $DyCo_3$ and amorphous $TbCo_3$ is reduced to ∼75% of the $4f$ atomic moment by the noncollinear magnetic structures attributed principally to random uniaxial magnetic anisotropy at the rare-earth sites and a negative sign of the quadrupole moment of the $4f$ charge distribution. Below 50 K, higher-order terms in the local crystal field interaction varying as J_z^4 and J_z^6 reduce the strength of the easy-axis anisotropy and the sperimangnetic cone angle θ_0. The angle is also reduced by thermal excitations, but the magnetic structure only approaches collinear ferrimagnetism at temperatures well above 300 K for Dy and >300 K for Tb. The rare-earth moments in these random easy-axis rare-earth systems become Ising-like at low temperatures in the absence of exchange, with admixtures of $M_J = J$, $J-2$, $J-4$, and $J-6$ in the ground state. Coercivity is large (≈3 T) because magnetization reversal is difficult to nucleate and coercivity tends to diverge with the anisotropy field at compensation. The spin-flop field of only 2 T for Dy is explained by the large transverse susceptibility of the frustrated noncollinear rare-earth subnetwork.

Amorphous $TmCo_3$ also exhibits compensation, but the $4f$ quadrupole moment is positive, leading to random local hard-axis anisotropy, with easy directions in a perpendicular plane for each atom. Coercivity is small, and the resulting uniaxial anisotropy is only half as strong as it is in the random easy-axis case; there is no divergence at compensation. The sperimagnetic cone angle is smaller than it is for the easy-axis rare earths, and the low-temperature Tm moment is 85% of the atomic value. XY-like behavior at low temperature is modified by the off-diagonal second-order crystal field, which mixes $M_J = 2$ into the $M_J = 0$ ground state, favoring an axis in the perpendicular easy-plane and increasing θ_0.

The single-pulse optical partial toggle switching in 10 nm a-$DyCo_3$ is shown to be a stochastic process, unrelated to defects in the thin film, which requires increasing laser energy as the Dy anisotropy increases at low temperatures. The sperimagnetic domain size appears to be set by the perpendicular magnetic anisotropy.

A remaining open question is whether the ground-state magnetic structure evolves continuously from weak to strong pinning as a function of α or whether there is an abrupt transition, as suggested by early small-scale computer simulations [60]. Another is the role of random anisotropy, rather the Dzyaloshinskii-Moria interaction, in favoring skyrmions in the weak-pinning limit [25,26].

ACKNOWLEDGMENTS

This work was supported by Science Foundation Ireland under Grants No. 16/IA/4534 ZEMS, No. 12/RC/2278 AMBER, and No. 17/NSFC/5294 MANIAC and EU FET Open Grant No. 737038 TRANSPIRE. K.S. acknowledges a postdoctoral fellowship from the Humboldt Foundation. Z.H. acknowledges support of a postgraduate scholarship from Trinity College Dublin. The authors thank the Helmholtz-Zentrum Berlin for the provision of access to synchrotron radiation facilities and allocation of synchrotron radiation at SPEEM end-station of UE46-PGMa beamline. We are grateful to Florian Kronast and Alevtina Smekhova for support during the synchrotron experiment and to Yangkun He and Lucy Prendeville for help with magnetization measurements.

DATA AVAILABILITY

Data are available upon reasonable request from the authors. Raw data and associated metadata recorded at the HZB will become available under the Creative Commons CC0 Dedication five years after publication.

[1] W. E. Wallace, *Rare Earth Intermetallics* (Academic Press, New York, 1973).

[2] K. Buschow, Intermetallic compounds of rare-earth and 3*d* transition metals, Rep. Prog. Phys. **40**, 1179 (1977).

[3] J. M. D. Coey, *Rare-Earth Ion Permanent Magnets* (Oxford University Press, Oxford, 1996).

[4] P. Hansen, Magnetic amorphous alloys, Handb. Magn. Mater. **6**, 289 (1991).

[5] J. M. D. Coey, Amorphous magnetic order, J. Appl. Phys. **49**, 1646 (1978).

[6] M. Mansuripur, *The Physical Principles of Magneto-Optical Recording* (Cambridge University Press, Cambridge, 1995).

[7] P. Hansen, C. Clausen, G. Much, M. Rosenkranz, and K. Witter, Magnetic and magneto-optical properties of rare-earth transition-metal alloys containing Gd, Tb, Fe, Co, J. Appl. Phys. **66**, 756 (1989).

[8] C. D. Stanciu, F. Hansteen, A. V. Kimmel, A. Kirilyuk, A. Tsukamoto, A. Itoh, and T. Rasing, All-optical magnetic recording with circularly polarized light, Phys. Rev. Lett. **99**, 047601 (2007).

[9] T. Ostler, J. Barker, R. Evans, R. Chantrell, U. Atxitia, O. Chubykalo-Fesenko, S. El Moussaoui, L. Le Guyader, E. Mengotti, and L. Heyderman, Ultrafast heating as a sufficient stimulus for magnetization reversal in a ferrimagnet, Nat. Commun. **3**, 666 (2012).

[10] A. El-Ghazaly, B. Tran, A. Ceballos, C.-H. Lambert, A. Pattabi, S. Salahuddin, F. Hellman, and J. Bokor, Ultrafast magnetization switching in nanoscale magnetic dots, Appl. Phys. Lett. **114**, 232407 (2019).

[11] Z. Hu, J. Besbas, R. Smith, N. Teichert, G. Atcheson, K. Rode, P. Stamenov, and J. M. D. Coey, Single-pulse all-optical partial switching in amorphous Dy_xCo_{1-x} and Tb_xCo_{1-x} with random anisotropy, Appl. Phys. Lett. **120**, 112401 (2023).

[12] T.-M. Liu, T. Wang, A. H. Reid, M. Savoini, X. Wu, B. Koene, P. Granitzka, C. E. Graves, D. J. Higley, and Z. Chen, Nanoscale confinement of all-optical magnetic switching in TbFeCo-competition with nanoscale heterogeneity, Nano Lett. **15**, 6862 (2015).

[13] Y. Liu, H. Cheng, P. Vallobra, H. Wang, S. Elmer, X. Zhang, G. Malinowski, M. Hehn, Y. Xu, S. Mangin *et al.*, Ultrafast single-pulse switching of Tb-dominant CoTb alloy, Appl. Phys. Lett. **122**, 022401 (2022).

[14] S. Tsunashima, S. Masui, T. Kobayashi, and S. Uchiyama, Magneto-optic Kerr effect of amorphous Gd-Fe-Co films, J. Appl. Phys. **53**, 8175 (1989).

[15] S. Uchiyama, Magnetic properties of rare earth–cobalt amorphous films, Mater. Chem. Phys. **42**, 38 (1995).

[16] P. Hansen, S. Kahn, C. Clausen, G. Much, and K. Witter, Magnetic and magneto-optical properties of rare-earth transition-metal alloys containing Dy, Ho, Fe, Co, J. Appl. Phys. **69**, 3194 (1991).

[17] J. M. D. Coey, J. Chappert, J. Rebouillat, and T. Wang, Magnetic structure of an amorphous rare-earth transition-metal alloy, Phys. Rev. Lett. **36**, 1061 (1976).

[18] Z. Hu, J. Besbas, K. Siewierska, R. Smith, P. Stamenov, and J. M. D. Coey, Magnetism, transport and atomic structure of amorphous binary Y_xCo_{1-x} alloys, Phys. Rev. B **109**, 014409 (2024).

[19] K. G. Balymov, E. V. Kudyukov, V. O. Vas'kovskiy, O. A. Adankova, N. A. Kulesh, E. A. Stepanova, and A. S. Rusalina, Magnetism of amorphous Dy-Tb-Co-type films, J. Phys. Conf. Series **1389**, 012014 (2019).

[20] R. Hussain, Aakansha, B. Bhrama, R. K. Basumatary, R. Bhrama, S. Ravi, and S. K. Shrivastava, Sperimagnetism in perpendicularly magnetized Co-Tb alloy-based thin films, J. Supercond. Nov. Magn. **32**, 4027 (2019).

[21] V. O. Vas'kovskiy, E. V. Kudyukov, E. A. Stepanova, E. A. Kravtsov, O. A. Adankova, A. S. Rusalina, K. G. Balymov, and A. V. Svalov, Experimental study and modeling of the magnetic properties of Dy-Co films, Phys. Metals Metallogr. **122**, 478 (2021).

[22] K. Chen, D. Lott, F. Radu, F. Choueikani, E. Otero, and P. Ohresser, Temperature-dependent magnetic properties of ferrimagnetic $DyCo_3$ alloy films, Phys. Rev. B **91**, 024409 (2015).

[23] D. H. Suzuki, M. Valvidares, P. Gargiani, M. Huang, A. E. Kossak, and G. S. D. Beach, Thickness and composition effects on atomic moments and magnetic compensation point in rare-earth transition metal thin films, Phys. Rev. B **107**, 134430 (2023).

[24] D.-H. Kim, M. Haruta, H.-Y. Ko, G. Go, H.-J. Park, T. Nishimura, D.-Y. Kim, T. Okno, Y. Hirata, H. Yoshikawa *et al.*, Bulk Dzyaloshinskii-Moriya interaction in amorphous ferrimagnetic alloys, Nat. Mater. **18**, 685 (2019).

[25] K. Chen, D. Lott, A. Philppi-Kobs, M. Weigrand, C. Luo, and F. Radu, Observation of compact ferrimagnetic skyrmions in a $DyCo_3$ film, Nanoscale **12**, 18137 (2020).

[26] C. Luo, K. Chen, V. Ukleev, S. Wintz, M. Weigand, R.-M. Abrudan, K. Prokeš, and F. Radu, Direct observation of Néel-type skyrmions and domain walls in a ferrimagnetic $DyCo_3$ thin film, Commun. Phys. **6**, 218 (2023).

[27] S. K. Kim, G. S. D. Beach, K-J. Lee, T. Ono, T. Rasing, and H. Yan, Ferrimagnetic spintronics, Nat. Mater. **21**, 24 (2022).

[28] Y. Kakehashi and M. Yu, Metallic magnetism in amorphous Co-Y alloys, Phys. Rev. B **49**, 15076 (1994).

[29] K. Fukamichi, T. Goto, and U. Mizutani, The crystallization temperature, electrical resistivity and magnetic properties of Co-Y amorphous alloys, IEEE Trans. Magn. **23**, 3590 (1987).

[30] J. M. D. Coey, *Magnetism and Magnetic Materials*, 2nd ed. (Cambridge University Press, Cambridge, 2025).

[31] G. Adachi and N. Imanaka, The binary rare earth oxides, Chem. Rev. **98**, 1479 (1998).

[32] D. Hou, Y. Li, D. Wei, L. Wu D.Tian, and X. Jin, The anomalous Hall effect in epitaxial face-centered-cubic cobalt films, J. Phys.: Condens. Matter **24**, 482001 (2012).

[33] R. Asomoza, I. A. Campbell, H. Jouve, and R. Meyer, Extraordinary Hall effect in rare-earth–cobalt amorphous films, J. Appl. Phys. **48**, 3829 (1977).

[34] N. T. Hai, J.-C. Wu, J.-P. Chou, and J. Pothan, Novel anomalous Hall effect mechanism in ferrimagnetic Gd-Co alloys, J. Appl. Phys. **133**, 233901 (2023).

[35] See Supplemental Material at http://link.aps.org/supplemental/10.1103/yzfd-jqvx for S1, partial single-pulse all-optical switching; S2, the soft component; S3, random anisotropy; S4, a-$TbCo_3$ data; S5, spin flop in a-Gd-Fe-Co; and which includes Refs. [61–67] and Tables S1 and S2.

[36] A. Gangulee and R. C. Taylor, Mean field analysis of the magnetic properties of vapour deposited amorphous Gd-Fe thin films, J. Appl. Phys. **49**, 1762 (1978).

[37] R. W. Cochrane, R. Harris, and M. J. Zuckermann, The role of structure on the magnetic properties of amorphous alloys, Phys. Rep. **48**, 1 (1978).

[38] A. Fert and I. A. Campbell, Nonaxial electric field gradients in amorphous rare earth alloys, J. Phys. F: Met. Phys. **8**, L57 (1978).

[39] R. Harris, M. Plischke, and M. Zuckermann, New model for amorphous magnetism, Phys. Rev. Lett. **31**, 160 (1973).

[40] K. Moorjani and J. M. D. Coey, *Magnetic Glasses* (Elsevier, Amsterdam, 1986), pp. 266–298.

[41] J. M. D. Coey and S. von Molnar, Linear specific heat of on amorphous magnet due to single-ion excitations, J. Phys. Lett. **39**, 327 (1978).

[42] K. Wang, Z. Xu, and S. Dong, A simple method for tuning perpendicular magnetic properties of ultra-thin TbFeCo films, Mater. Lett. **236**, 89 (2019).

[43] B. Boucher, Bulk magnetic properties of the amorphous magnetic alloys $RE_{50}Ag_{50}$ (RE = Gd, Tb, Dy, Ho and Er), IEEE Trans. Magn. **13**, 1601 (1977).

[44] R. Asomoza, I. A. Campbell, A. Fert, A. Liénard, and J. P. Rebouillat, Magnetic and transport properties of nickel-rare earth amorphous alloys, J. Phys. F: Met. Phys. **9**, 349 (1979).

[45] A. K. Bhattacharjee, B. Coqblin, R. Jullien, and M. J. Zuckermann, Magnetic properties of amorphous metallic alloys containing rare-earth and transition metal components, Physica B+C **91**, 179 (1977).

[46] A. K. Bhattacharjee, R. Jullien, and M. J. Zuckermann, Magnetic properties of amorphous metallic alloys containing rare earth impurities, J. Phys. F: Met. Phys. **7**, 393 (1977).

[47] H. Zhang, D. Zeng, and Z. Liu, The law of approach to saturation in ferromagnets originating from the magnetocrystalline anisotropy, J. Magn. Magn. Mater. **322**, 2375 (2010).

[48] L. V. Pourovskii, J. Boust, R. Ballou, G. G. Eslava, and D. Givord, Higher-order crystal field and rare-earth magnetism in rare-earth-Co_5 intermetallics, Phys. Rev. B **101**, 214433 (2020).

[49] H. Fu, M. Mansuripur, and P. Meystred, Generic source of perpendicular anisotropy in amorphous rare-earth-transition-metal films, Phys. Rev. Lett. **66**, 1086 (1991).

[50] V. G. Harris, K. D. Aylesworth, B. N. Das, W. T. Elam, and N. C. Koon, Structural origins of magnetic anisotropy in sputtered amorphous Tb-Fe films, Phys. Rev. Lett. **69**, 1939 (1992).

[51] K. Srinivasan, Y. Chen, L. Cestarollo, D. K. Dare, J. G. Wright, and A. El-Ghazaly, Engineering large perpendicular magnetic anisotropy in amorphous ferrimagnetic gadolinium cobalt alloys, J. Mater. Chem. C **11**, 4820 (2023).

[52] E. Kirk, C. Bull, S. Finizio, H. Sepehri-Amin, S. Wintz, A. K. Suszka, N. S. Bingham, P. Warnicke, K. Hono, P. W. Nutter *et al.*, Anisotropy-induced spin reorientation in chemically modulated amorphous ferrimagnetic films, Phys. Rev. Mater. **4**, 074403 (2020).

[53] C. Fowley, K. Rode, Y.-C. Lau, N. Thiyagarajah, D. Betto, K. Borisov, G. Atcheson, E. Kampert, Z. Wang, Y. Yuan *et al.*, Magnetocrystalline anisotropy and exchange probed by high-field anomalous Hall effect in fully-compensated half-metallic Mn_2Ru_xGa thin films, Phys. Rev. B **98**, 220406(R) (2019).

[54] U. Kobler and A. Hoser, Spin flop transition in yttrium iron garnet, Solid State Commun. **142**, 350 (2007).

[55] J. Becker, A. Tsukamoto, A. Kirilyuk, J. C. Maan, Th. Rasing, P. C. M. Christianen, and A. V. Kimel, Ultrafast magnetism of a ferrimagnet across the spin-flop transition in high magnetic fields, Phys. Rev. Lett. **118**, 117203 (2017).

[56] R. C. Bhatt, L.-X. Ye, N. T. Hai, J.-C. Wu, and T.-H. Wu, Spin-flop led peculiar behavior of temperature-dependent anomalous Hall effect in Hf/Gd-Fe-Co, J. Magn. Magn. Mater. **537**, 168196 (2021).

[57] D. Chen, Y. Xu, S. Tong, W. Zheng, Y. Sun, J. Lu, N. Lei, D. Wei, and J. Zhao, Noncollinear spin state and unusual magnetoresistance in ferrimagnet Co-Gd, Phys. Rev. Mater. **6**, 014402 (2022).

[58] T. Huang, A study of the behavior and mechanism of all-optical switching, Doctoral thesis, University of Lorraine, 2023.

[59] C. Banerjee, N. Teichert, K. E. Siewierska, Z. Gercsi, G. Atcheson, P. Stamenov, K. Rode, J. M. D. Coey, and J. Besbas, Single-pulse all-optical toggle switching of the magnetization without Gadolinium in the ferrimagnet Mn_2RuGa, Nat. Commun. **11**, 4444 (2020).

[60] R. Alben, J. J. Becker, and M. C. Chi, Random anisotropy in amorphous ferromagnets, J. Appl. Phys. **49**, 1653 (1978).

[61] F. Kronast and S. V. Molina, SPEEM: The photoemission microscope at the dedicated microfocus PGM beamline UE49-PGMa at BESSY II, J. Large-scale Res. Facilities **2**, A90 (2016).

[62] A. Ceballos, M. Charilaou, M. Molina-Ruiz, and F. Hellman, Coexistence of soft and hard magnetic phases in single layer amorphous Tb-Co thin films, J. Appl. Phys. **131**, 033901 (2022).

[63] K. A. Thorarinsdóttir, B. R. Thorbjarnarsdóttir, U. B. Arnalds, and F. Magnus, Competing interface and bulk anisotropies in Co-rich TbCo amorphous films, J. Phys.: Condens. Matter **35**, 205802 (2023).

[64] J.-H. Park, W. T. Kim, W. Won, J.-H. Kang, S. Lee, B.-G. Park, B. S. Ham, Y. Jo, F. Rotermund, and K.-J. Kim, Observation of spin-glass-like characteristics in ferrimagnetic TbCo through energy-level selective approach, Nat. Commun. **13**, 5530 (2022).

[65] K. Wang, Y. Huang, Z. Xu, S. Dong, and R. Chen, Effect of sputtering power on the magnetic properties of amorphous TbFeCo films, J. Magn. Magn. Mater. **424**, 89 (2017).

[66] S. Zhang, Y. Zhang, L. Zhang, Z. Li, Y. Ren, Q. Jin, and Z. Zhang, Temperature dependence of magnetic properties in CoFe/Tb multilayers with perpendicular magnetic anisotropy, ACS Appl. Elec. Mater. **4**, 5361 (2022).

[67] A.-O. Mandru, O. Yıldırım, M. A. Marioni, H. Rohrmann, M. Heigl, O.-T. Ciubotariu, M. Penedo, X. Zhao, M. Albrecht, and H. J. Hug, Pervasive artifacts revealed from magnetometry measurements of rare earth-transition metal thin films, J. Vac. Sci. Technol. A **38**, 023409 (2020).